

# UC San Diego

## UC San Diego Electronic Theses and Dissertations

### Title

Anode Shape and Structure Effects on Dense Plasma Focus Neutron Yield

### Permalink

<https://escholarship.org/uc/item/12c9873v>

### Author

Eudave, Veronica

### Publication Date

2022

Peer reviewed|Thesis/dissertation

UNIVERSITY OF CALIFORNIA SAN DIEGO

Anode Shape and Structure Effects on Dense Plasma Focus Neutron Yield

A thesis submitted in partial satisfaction of the  
requirements for the degree of Master of Science

in

Engineering Sciences (Engineering Physics)

by

Veronica Eudave

Committee in charge:

Professor Farhat Beg, Chair  
Professor Alexey Arefiev  
Professor Olivia Graeve

2022

Copyright

Veronica Eudave, 2022

All rights reserved.

The thesis of Veronica Eudave is approved, and is acceptable in quality and form for publication on microfilm and electronically.

University of California San Diego

2022

## **Dedication**

Por mis padres que dejaron la comodidad de su comunidad para darles a sus hijos  
oportunidades que ellos nunca tuvieron.

For my brother who always believed in me.

For my sisters who I hope to inspire.

Para mi abuelita, quien me paso su alegria, locura, y quien me enseño que la  
puerta ni de cien candados van a poder a mi detenerme.

Veronica Eudave

## Epigraph

*There is a place with four suns in the sky – red, white, blue, and yellow; two of them are so close together that they touch, and star stuff flows between them. I know of a world with a million moons. I know of a sun the size of the Earth - and made of diamond. There are atomic nuclei a few miles across which rotate thirty times a second. There are tiny grains between the stars, with the size and atomic composition of bacteria. There are stars leaving the Milky Way, and immense gas clouds falling into it. There are turbulent plasmas writhing with X- and gamma-rays and mighty stellar explosions. There are, perhaps, places which are outside our universe. The universe is vast and awesome, and for the first time we are becoming a part of it.*

- Carl Sagan, *Planetary Exploration* (1970)

# Table of Contents

|   |      |
|---|------|
| Thesis Approval Page .....                        | iii  |
| Dedication .....                                  | iv   |
| Epigraph .....                                    | v    |
| Table of Contents .....                           | vi   |
| List of Abbreviations .....                       | viii |
| List of Symbols .....                             | ix   |
| List of Figures .....                             | x    |
| List of Tables .....                              | xii  |
| Acknowledgements .....                            | xiii |
| Vita .....  | xiv  |
| Abstract of the Thesis .....                      | xv   |
| 1. Introduction .....                             | 1    |
| 1.1. Past Experiments .....                       | 4    |
| 1.2. Motivation .....                             | 6    |
| 1.3. Research Objectives .....                    | 8    |
| 2. Methods .....                                  | 9    |
| 2.1. Experimental Set Up .....                    | 9    |
| 2.2. Multi-gap Multi-Channel Switch .....         | 12   |
| 2.3. Anodes .....                                 | 13   |
| 2.4. Diagnostics .....                            | 15   |
| 2.4.1. Be-activation Detector .....               | 15   |
| 2.4.2. Schlieren and Time Integrated Images ..... | 17   |

|   |    |
|---|----|
| 2.4.3. AXUV Diodes.....                         | 18 |
| 3. Results and Discussion .....                 | 19 |
| 3.1. Neutrons.....                              | 19 |
| 3.2. Schlieren and Time Integrated Images ..... | 22 |
| 3.2.1. Pinch Dynamics .....                     | 25 |
| 4. Conclusions.....                             | 28 |
| 4.1. Future Work.....                           | 28 |
| References.....                                 | 30 |



## List of Abbreviations

|      |  |
|------|--|
| AXUV | Absolute XUV                                   |
| BDL  | Below Detection Limit                          |
| DPF  | Dense Plasma Focus                             |
| GM   | Geiger-Milller                                 |
| ICF  | Inertial Confinement Fusion                    |
| MCS  | Multichannel Scaler                            |
| MHD  | Magnetohydrodynamic                            |
| MSTS | Mission Support and Test Services              |
| NASA | National Aeronautics and Space Administration  |
| NIST | National Institute of Standards and Technology |
| PMT  | Photomultiplier Tube                           |
| UCSD | University of California San Diego             |
| XUV  | Extreme Ultraviolet Radiation                  |

## List of Symbols

|               |                            |
|---------------|----------------------------|
| Al            | Aluminum                   |
| Be            | Beryllium                  |
| cm            | Centimeters                |
| Cu            | Copper                     |
| He            | Helium                     |
| I             | Current                    |
| in            | Inches                     |
| $k_b$         | Boltzmann's constant       |
| kJ            | kilo Joules                |
| kV            | kilo Volts                 |
| L             | Inductance                 |
| $\mu_0$       | Permeability of Free Space |
| $\mu\text{m}$ | Microfarads                |
| $\mu\text{m}$ | Micrometer                 |
| N             | Density                    |
| Ne            | Neon                       |
| nH            | Nanohenry                  |
| V             | Voltage                    |
| $T_e$         | Mean Electron Temperature  |
| $T_i$         | Mean Ion Temperature       |
| z             | Ionic charge number        |

# List of Figures

|  |    |
|--|----|
| Figure 1-1. Nine different z-pinch configurations that use different materials to achieve implosion. Some materials include wire arrays and gas puffs [2] .....  | 3  |
| Figure 1-2. The three stages of a DPF implosion: Initiation Phase, Axial Rundown Phase, and Radial Implosion Phase. In the Initiation Phase, the plasma sheath is lifted off the insulator sleeve using JxB forces. In the Axial Rundown Phase, the sheath gathers more material as it snowplows and is pushed by JxB forces.....  | 4  |
| Figure 1-3. MHD pinch simulations done by Appelbe and Chittenden [6] demonstrating pinch dynamics with different anodes. The images in which there is an anode with a hollow, the pinch is seen developing and extending within the hollow. For the anode that does not have a hollow, a symmetric pinch with minimal instabilities begins to form at the tip of the anode ..... | 7  |
| Figure 2-1. a) Schematic of anode with labels and an integrated image of a pinch using the hemispherical hollow. b) Graph with current and voltage traces and c) diode signals using a 12.5 $\mu\text{m}$ Cu and a 45 $\mu\text{m}$ Al filters .....   | 9  |
| Figure 2-2. a) DPF vacuum chamber c) capacitor bank, b) anode and cathode assembly and d) close up of anode with the hemispherical hollow anode installed.....   | 11 |
| Figure 2-3. a) Multi-channel, multi-gap spark gap in its place under the vacuum chamber and b) taken out and in need of refurbishing. Oil deposits from the switch pump cover the inside of the switch .....   | 13 |
| Figure 2-4. The hemispherical hollow, hemispherical solid, and flat top slit hollow anodes along with their defining symbols, CAD drawings, and dimensions. Each anode is made of copper and is 4.25 inches in length and has an outer diameter of 1.22 inches. The hollows have a diameter of 0.6 inches .....  | 15 |
| Figure 2-5. Be-activation detector designed by MSTs and cross-calibrated at the Ion Beam Lab in Sandia National Lab and placed directly outside of the vacuum chamber. A graphical example of a decay in bin counts in MCS data is shown .....   | 16 |
| Figure 2-6. "Upper" and "lower" Schlieren images of an experiment for each anode. The "lower" Schlieren image is the rundown phase in which we see the plasma sheath lift off. The upper Schlieren image is that which captures the top of the anode in which the pinch occurs. The anode is outlined to promote visibility.....   | 17 |
| Figure 2-7. Transmission curves for 12.5 $\mu\text{m}$ Cu and 45 $\mu\text{m}$ Al filters from Henke Gas Transmission Website [13] .....   | 18 |
| Figure 3-1. Maximum neutron yield per anode (top) at a pressure range from 3 torr to 8 torr as well as their corresponding neutron averages and standard deviations (bottom) .....   | 20 |

Figure 3-2. Images of a pinch occurring with each anode at a pressure of 5 torr. The pinch that forms with the hollow anodes moves in the axial direction as it is channeled by the hollow. The bright light that forms at the tip of hemispherical solid anode is asymmetric and is believed to be copper ablation. This is corroborated by X-ray data that is for future work on this DPF ..... 22

Figure 3-3. Schlieren images of well-timed pinches for each anode as well as corresponding time evolution images. The anode and cathode rods are outlined to improve visibility. The ideal pinch is one that has minimal instabilities and a uniform and dense column is produced at the tip of the anode ..... 24

Figure 3-4. Close up images of tip of each anode to see the dynamics of the pinch formation. The hemispherical hollow anode found has a symmetric pinch while the hemispherical solid does not form a pinch. The flat top hollow anode with slits shows plasma activity inside of the hollow. In the close up image, one can see the pinch extending into the hollow ..... 26

## **List of Tables**

Table 2-1. Symbols used to identify each anode in this thesis and their characteristics ..... 14

## **Acknowledgements**

I would first like to thank Professor Farhat Beg for allowing me the opportunity of joining his group which has in turn opened the door for many opportunities. I would also like to thank Drs. Eric N Hanh and Fabio Conti for teaching me everything that I know about lab work and for not giving up on me. A special thanks to Dr. Maria Pia Valdivia for being a great mentor, friend and for always believing in me and a warm thanks to Jacquelynne Vaughan for being my at work therapist and confidant. Last but certainly not least, I would like to thank the members of my committee; Professor Alexey Arefiev for being a great professor and genuinely cared about your students; Professor Olivia Graeve for allowing me the chance to have a coffee with her over two years ago and encouraging me to apply to graduate school.

This project has been supported by the Air Force Office of Scientific Research announcement FA9550-18-S-0003.

This thesis, in part is currently being prepared for submission for publication of the material. Eudave, Veronica; Hahn, Eric N.; Valdivia, Maria Pia; Vaughan, Jacquelynne; Ghosh, Swarvanu; Conti, Fabio; Beg, Farhat, N. The thesis author was the primary investigator and author of this material.

## **Vita**

2020 B.S. Aerospace Engineering - University of California San Diego

2022 M.S. Engineering Sciences (Engineering Physics) - University of California San Diego

## **Publications**

E. N. Hahn, S. Ghosh, V. Eudave, J. Narkis, J. R. Angus, A. J. Link, F. Conti, F. N. Beg. "Effect of Insulator Length and Fill Pressure on Filamentation and Neutron Production in a 4.6 kJ Dense Plasma Focus." *Phys. Plasmas*. (2022) 12.

# **Abstract of the Thesis**

Anode Shape and Hollow Effects on Dense Plasma Focus Neutron Yield

by

Veronica Eudave

Master of Science in Engineering Sciences (Engineering Physics)

University of California San Diego, 2022

Professor Farhat Beg, Chair

The Dense Plasma Focus (DPF) is a simple z-pinch device with the ability of producing X-rays and neutrons. Neutron production from a DPF is susceptible to electrical parameters such as voltage and current, as well as mechanical parameters including electrode geometry and



insulator sleeve length. Experiments that investigate three different anode geometries on a 4.6 kJ DPF device with a voltage of -20 kV and a current of -230kA were carried out. Two anodes with a hemispherical tip, one with and one without a hollow, were explored as well as an anode with a flat tip, hollow, and concentric slits. In order to analyze the pinches produced in these experiments, a neutron activation detector, X-ray PIN diodes, and a series of time-resolved Schlieren probing, were used. Hollow anodes create a higher neutron yield based on recent magnetohydrodynamics simulations that show the extension and dynamics of pinches in the hollow structure. Experimental evidence of extension of the pinch column is shown for the first time using the flat top hollow anode with slits. The maximum neutron yield obtained in these experiments was  $1.97 \pm 0.1 \times 10^8$  neutrons per pulse which was acquired using the hemispherical hollow anode while hard X-ray emission was observed with the hemispherical solid anode. Based on this analysis, one can conclude that anode with a hollow is optimal for neutron production while one without a hollow is prone to ablation and serves as an X-ray source.

Research supported by Air Force Office of Scientific Research grant FA9550-18-S0003.

# 1. Introduction

The desire for knowledge about our universe and the ability to make day to day life more efficient has always been instinctively human. The origins of the universe and innovative technological and energy reform are investigated by two separate communities with distinct backgrounds. These two philosophies, however different they may seem, in many ways go hand in hand. Technology is taking a leap forward and individuals are looking for more ecofriendly and cost effective ways to make our lives more comfortable while continuing to battle the negative environmental changes happening on our Earth. On the other hand, in order to understand the universe and its origins, we must understand what it is made of. According to NASA's Dr. Dennis Gallagher, 99% of the universe is made of plasma. To our convenience, plasma has shown to be a feasible energy source and an excellent electrical conductor. Plasma, the fourth state of matter, is a gas that has been heated to the point where partial-ionization of the gas occurs and electrons are separated and released from its prior molecule or atom. It is a natural phenomenon that occurs from the outermost corner of the universe - where Voyager 1 is currently floating around - all the way to Iceland where the aurora borealis dances during winter nights. It has enthralled scientists for years and human-made plasmas are now common in laboratory setting. The presence of free electrons and ions in plasma allow the material to act as a conductor for current and electricity to pass through [1]. This advantageous property is what has sparked interest in studying plasmas in order to fully grasp its abilities and potentially make use of its benefits in day to day life. Facilities around the world are attempting to find a way to optimize fusion in order to use the energy produced by these devices as an alternative and cleaner energy source.

The two major fusion confinement processes that are widely studied are magnetic and inertial confinement (ICF). The formation of plasma in these processes is accomplished due to an

applied magnetic field or inertia, respectively. However, there are a variety of smaller devices that adopt different characteristics from these two confinement methods to approach fusion such as a z-pinch machine. The z-pinch is a confinement process in which a high current is passed through a gas which leads to the development of a self-generating magnetic field [2]. There are various types of z-pinches which include: compressional z-pinch, gas-puff z-pinch, wire-array z-pinch, hohlraums and more which are shown in Figure 1-1 [2]. A uniform z-pinches are described by the Bennett relation which was first developed in 1934 as a way to describe the stream of particles with a uniform axial velocity [3]. The type of z-pinch configuration investigated in this thesis is the Dense Plasma Focus.

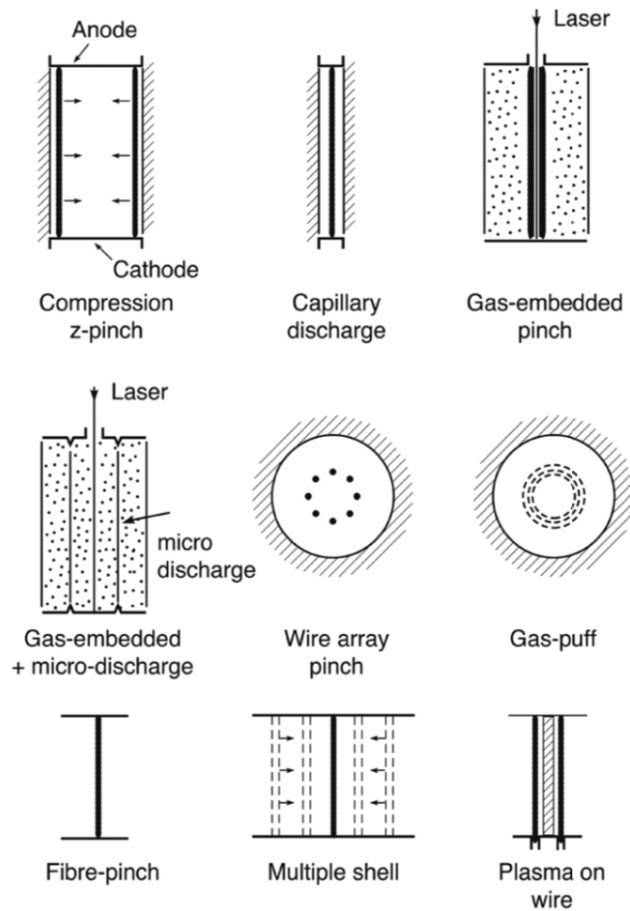


Figure 1-1. Nine different Z-pinch configurations that use different materials to achieve implosion. Some materials include wire arrays and gas puffs [2].

The Dense Plasma Focus, also known as DPF, is a simple z-pinch configuration first developed in the USSR by N.V. Fillipov [4] and then later introduced in the United States by J. W. Mather in the 1960s [5]. The DPF is an intense source of energetic particles (electrons, ions and neutrons) and radiation (soft and hard X-rays) as it does not require a large and complex set up to maximize its neutron production rates [6]. A typical DPF consists of a central anode surrounded by concentric cathode rods which are separated by an insulator sleeve. There are three distinct phases of a DPF experiment that ultimately lead to a hot plasma column as seen in Figure 1-2. The first is the initiation phase in which a breakdown takes place across the insulator sleeve

and plasma sheath lifts. The second is the axial rundown phase in which the plasma sheath is pushed in the axial direction by  $\mathbf{J}_z \times \mathbf{B}_0$  forces towards the end of the anode. In the final phase, the sheath moves inwards and pinches at the top of the anode creating a hot dense plasma column [7].

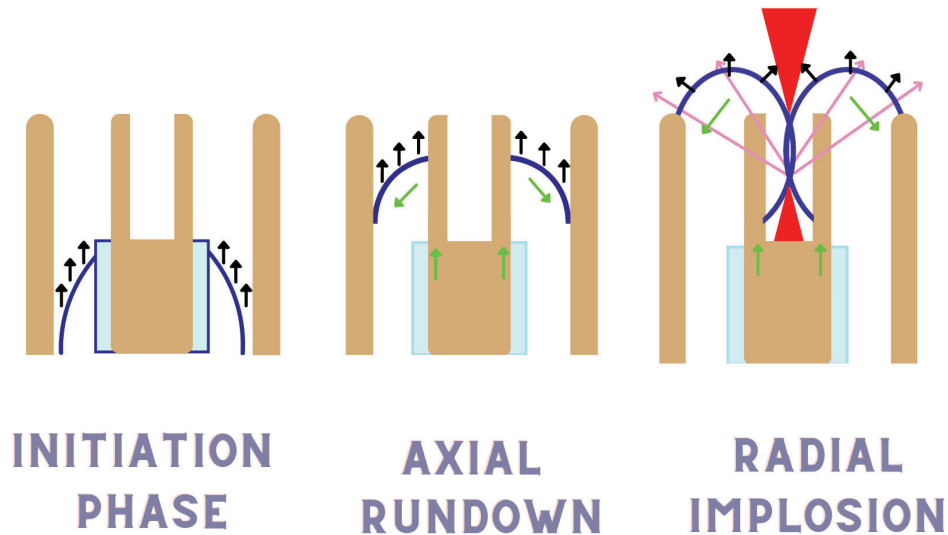


Figure 1-2. The three stages of a DPF implosion: Initiation Phase, Axil Rundown Phase, and Radial Implosion Phase. In the Initiation Phase, the plasma sheath is lifted off the insulator sleeve using  $\mathbf{J} \times \mathbf{B}$  forces. In the Axial Rundown Phase, the sheath gathers more material as it snowplows and is pushed by  $\mathbf{J} \times \mathbf{B}$  forces. The final phase, the sheath turns inwards and radially implodes.

### 1.1. Past Experiments

A study by B.H. Shaw *et al.* [8] addressed the effects of anode shape by placing their attention on the influence of hollow characteristics. Shaw examined seven anodes with the same overall geometry but with central cavities with different diameters that ranged from 0 to 1 inch. When the maximum neutrons produced for each of these anodes with a consistent pressure of 1.3 torr was compared using an  $^3\text{He}$  detector, it was found that there was an optimal hollow diameter that produced the overall highest neutron yield of  $9.1 \pm 0.4 \times 10^6$  neutrons per discharge. In their experiment, the hollow diameter that produced the highest neutron yield was that of 0.75 inches while poorest performing anode with respect to neutron production was the anode without any central cavity. In addition to neutron yields, Shaw also observed copper

sputtering in these anodes. By installing an on-axial target in their chamber, they were able to measure the copper that was expelled from the tip of each of the anodes. It was found that the smaller the hollow, the more damaged was observed on the anodes and a higher concentration of copper on the on-axial targets was measured which directly related copper sputtering to hollow scaling.

Hussain *et al.* [9] took a different approach than Shaw's by focusing their investigation on the shape of anode tip. They used two cylindrical anode configurations with the same size hollow but with distinct geometries, particularly, a tapered and flat top model. Based on their silver foil activated GM tube, they found a quantitative measurement for neutron yield which showed that the tapered anode produced the highest yield overall with a maximum average of  $1.6 \times 10^8$  neutrons per shot. The highest neutron yield Hussain *et al.* was able to qualitatively support this with integrated images of neutron emission zones which show the elongated pinch of that tapered anode which meant better compression. This study not only compared the neutron production between these two anode types, but also looked at the pinch energy of produced by each anode. Hussain used a Rogowski coil and high voltage probe to see how much energy was transferred into the pinch using each anode. He found that that the tapered anode transferred the energy more efficiently into the pinch and in return produced higher neutron yields than the flat top anode.

Each aspect of the central anode (hollow and tip shape) has an effect on neutron yield; however, differences may be seen when configured with different hollow-shape permutations. Talukdar *et al.* [10] tested one of these permutations by testing two anodes without central cavities with similar flat and converging tip shapes to those that Hussain *et al.* examined using a bubble dosimeter and photomultiplier tube (PMT) detectors. This paper, however, showed

results contrary to Hussain *et al.* Their research showed that the total neutron yield is lower in the tapered anode than the cylindrical anode with the flat top. In this set up, Talukdar *et al.* used anodes without a central cavity which in turn created drastic differences to the neutron yields. They also found that the anode that performed the best was not the tapered end anode like Hussain *et al.* used but the flat top anode. This anode had a typical average neutron yield of  $8.27 \times 10^6$  neutrons per shot in the axial direction and  $6.59 \times 10^6$  neutrons per shot in the radial direction. Although they found that the neutron energies were higher for that of the converging anode, neutron yields were less than that of the cylindrical flat top anode. They also found that the X-ray emission is higher for the converging anode. Their conclusion is that the beam target mechanism is the biggest contributor to neutron production in their device and that erosion of the anode tip plays an important part as well.

## 1.2. Motivation

For this study, we are particularly interested in the impact that anode geometry has on DPF experiments and the resulting X-rays and charged particles. Researchers have already started to observe effects that different anode geometry and hollow configurations have on DPF particle and radiation yields. Appelbe and Chittenden [6] for example, recently published research on optimization methods to improve and further understand how the DPF works. They produced magnetohydrodynamic (MHD) simulations using the GORGON [11] code of the pinch dynamics in a DPF with various anode configurations which are seen in Figure 1-3. These simulations show how a pinch would form around an anode with a hemispherical tip and a flat tip with a central cavity.

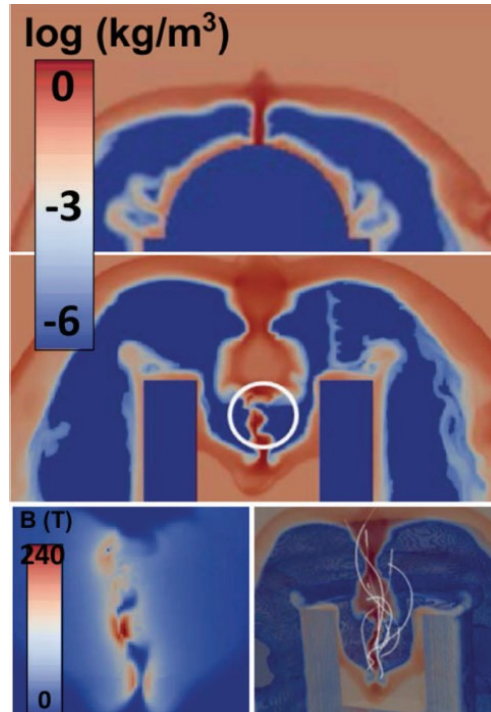


Figure 1-3. MHD pinch simulations done by Appelbe and Chittenden [6] demonstrating pinch dynamics with different anodes. The images in which there is an anode with a hollow, the pinch is seen developing and extending within the hollow. For the anode that does not have a hollow, a symmetric pinch with minimal instabilities begins to form at the tip of the anode.

Based on the simulations, anode geometry is a dictating factor on whether a structured pinch may form or if it is prone to instabilities. Their goal is to catalyze further investigation on the physical effects that the anode shape of a DPF can have on pinch production in order to find a way to optimize beam-target neutron production. This involves attempting a variety of anode configurations that may involve different permutations of tip and hollow shape as well as different hollow diameters.



### 1.3. Research Objectives

The purpose of this research is to identify what factors of the central anode contribute to the enhancement of the neutron yield by answering the following questions:

- How does the presence of a hollow and the shape of the anode affect pinch dynamics?
- Is there plasma activity within the anode hollow?
- Is there a configuration that tends to ablate more material?
- If the above is true, does that affect neutron yield?

This is done by analyzing neutron data, Schlieren and integrated images of the pinch for each anode at the same experimental parameters and at a pressure range of 3.0 torr to 8.0 torr.

## 2. Methods

### 2.1. Experimental Set Up

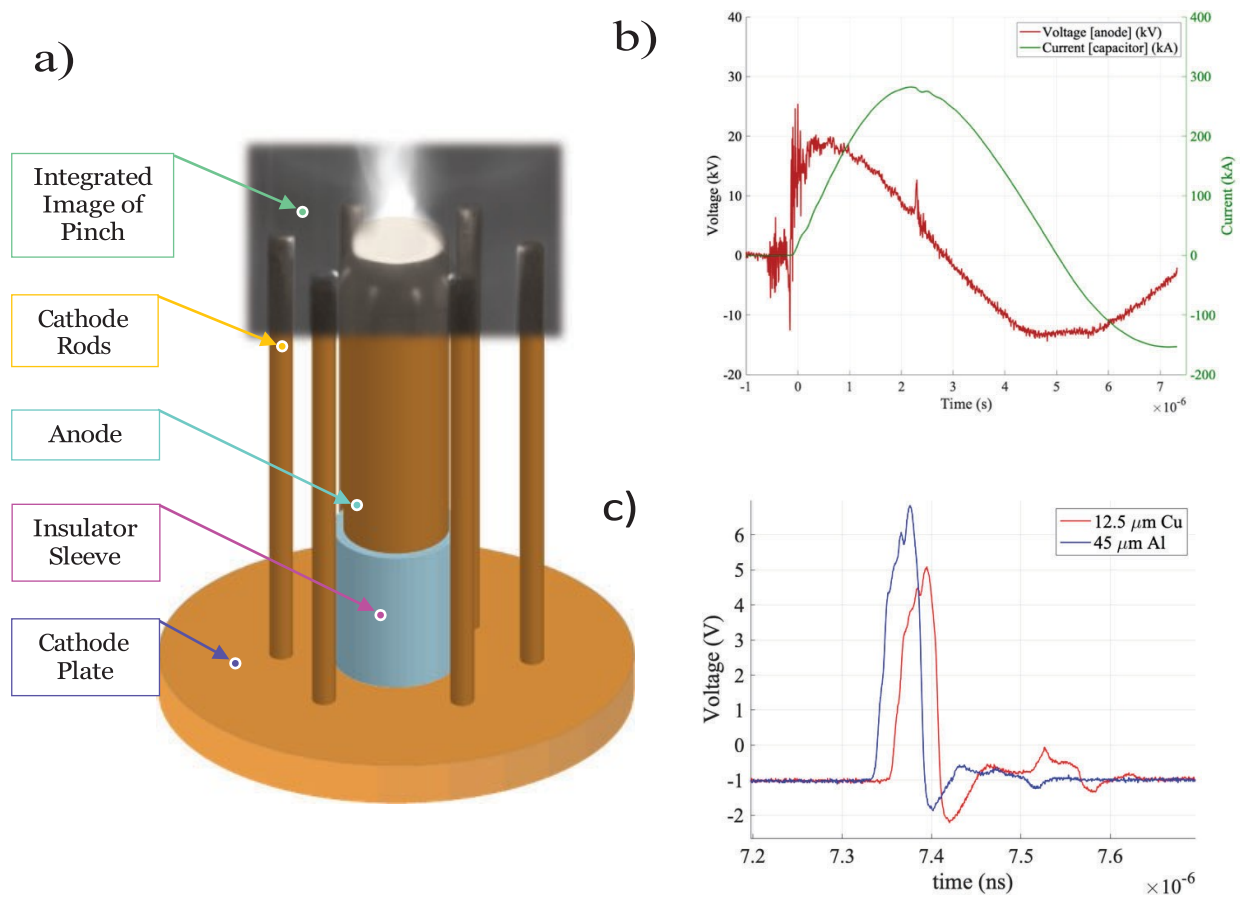


Figure 2-1. a) Schematic of anode with labels and an integrated image of a pinch using the hemispherical hollow. b) Graph with current and voltage traces and c) diode signals using a 12.5  $\mu\text{m}$  Cu and a 45  $\mu\text{m}$  Al filters.

UC San Diego's 4.6 kJ DPF operates at a voltage of 21 kV, an inductance of 110 nH, and a capacitance 20  $\mu\text{F}$ . The vacuum chamber that encases the electrode assembly is filled with deuterium of pressures ranging from 3.0 to 8.0 torr. The copper electrode assembly consists of 6 cathode rods, a central anode and a borosilicate insulator sleeve. The insulator

sleeve that is used is 3.56 cm long which was found to be the optimal length for neutron production in a previous study [12]. Figure 2-1a) shows a schematic of this electrode assembly with an integrated image of a pinch from an experiment using a hemispherical hollow anode well current and voltage traces (Figure 2-1b) and X-ray diode data (Figure 2-1c). Figure 2-2 shows pictures of the machine set up in the UCSD DPF lab. Figure 2-2a) shows the DPF vacuum chamber with multiple ports that that connect various diagnostics, a Rogowski coil, a pumping vacuum, and pressure gauge. Under the chamber, there is a large capacitive driver which is seen in Figure 2-2c) that is apply 21 kV of volts. Figure 2-2b) and Figure 2-2d) show the electrode assembly within the chamber as seen from one of the open ports.

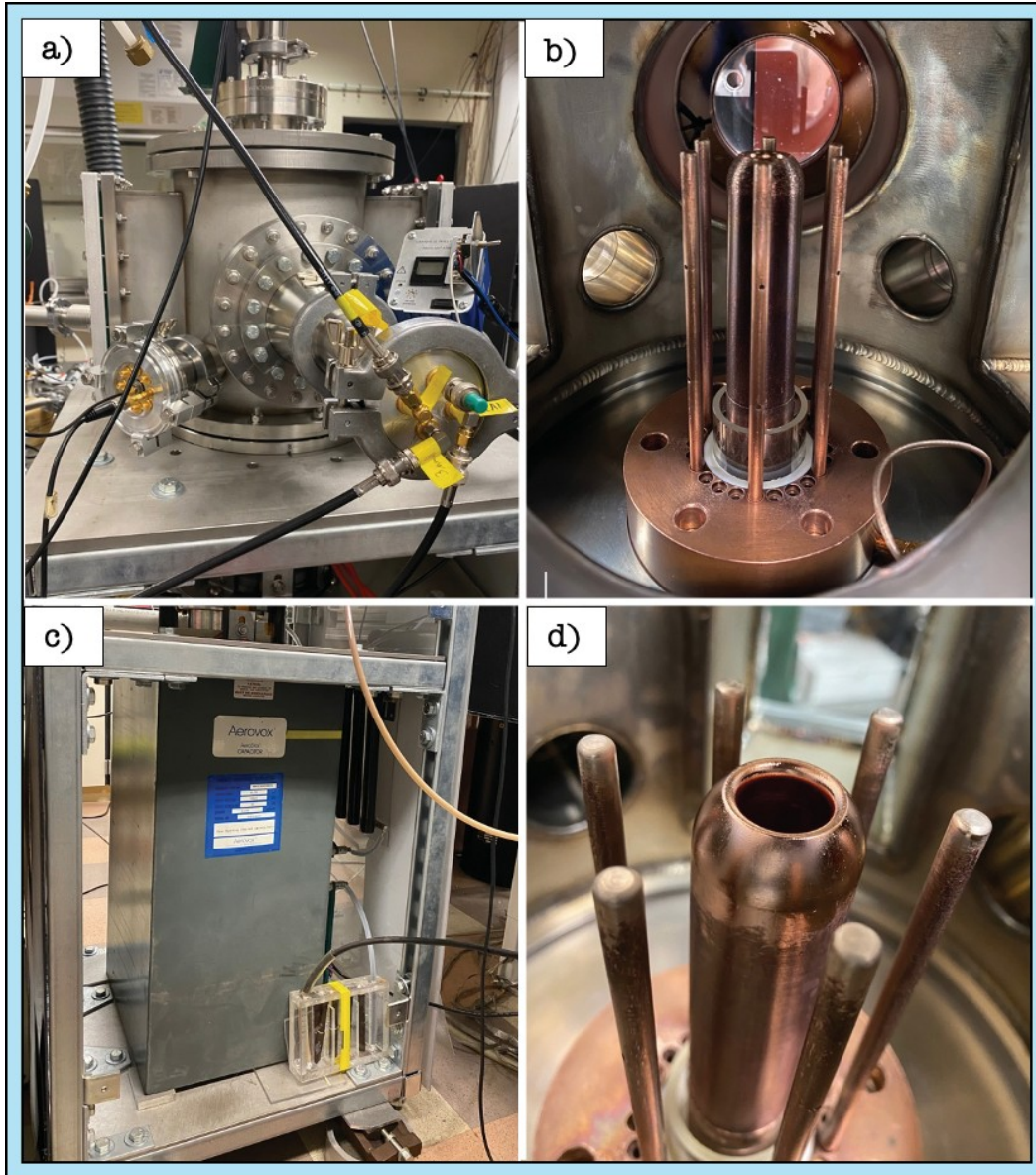


Figure 2-2. a) DPF vacuum chamber c) capacitor bank, b) anode and cathode assembly and d) close up of anode with the hemispherical hollow anode installed.

The experimental procedure for each anode starts by taking a minimum a series of shots at the optimal neutron producing pressure. This is done in order to prime the anodes since they are freshly fabricated and tend to ablate copper instead of giving significant data in the first rounds of shots. The pressure is determined based on the optimal pressure from previous experiments done with our DPF. Once neutrons begin to appear, we gather data from the

AXUV diodes, Be-detector, and Schlieren images at this pressure and move on to the upper and lower limit pressure, 3.0 and 8.0 torr. We start at these limits in order to get an estimate of the neutron limits we expect and then move on to the remaining pressures. Based on the previous experiments that explored the effects of anode shape and hollow presence, having a hollow and having a tapered end seemed to perform the best therefore the first anode installed in this experiment was the hemispherical hollow anode. After running experiments with each of these anodes, we returned to pressures in which we did not gather enough significant data to fill any holes in our data set.

## **2.2. Multi-gap Multi-Channel Switch**

The DPF has a multi-gap, multi-channel spark gap that is used to send the electrical current into the vacuum chamber. As seen in Figure 2-3a), the switch is found under the vacuum chamber and is made of two steel and copper plates at each end and contains two copper rings that have the ability to hold up 12 spherical electrodes on each ring. There are multiple grating resistors connected to channels of the switch which transfer the current up into the electrodes.

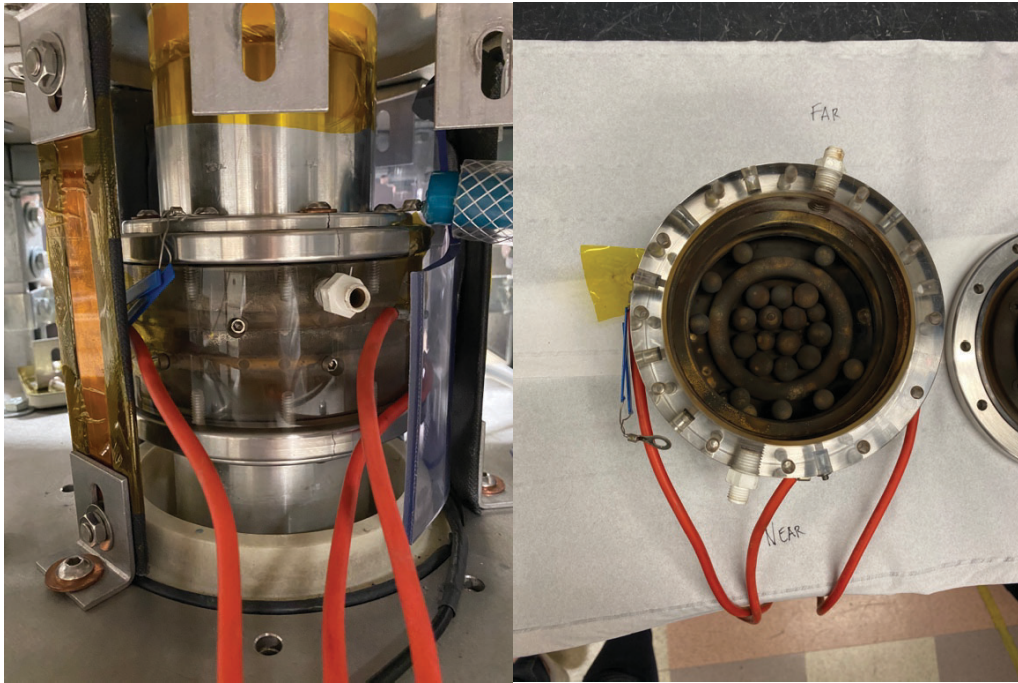


Figure 2-3. a) Multi-channel, multi-gap spark gap in its place under the vacuum chamber and b) taken out and in need of refurbishing. Oil deposits from the switch pump cover the inside of the switch.












This switch design has been used in our lab for past experiments, however, it has proven to not be the most effective design. The switch lifespan depends on a variety of factors that depend on the reliability of the spherical electrode attachments and the amount of oil deposits in the switch that come its vacuuming pump. Figure 2-3a) shows the switch removed from its place in the machine and in need of refurbishing. This is an involved and lengthy process that must be done once the triggering becomes faulty and is no longer firing during experiments. Implementing a new switch design that would address these issues and lengthen its lifespan would be an ideal next step in optimizing the DPF.

### 2.3. Anodes

The three copper anodes that are the focal point of our study are the 1) hemispherical top hollow anode, 2) hemispherical top solid anode, and 3) flat top hollow anode with slits

which are seen in Figure 2-4. Each of the anodes are 4.25 inches in length have an outer diameter of 1.22 inches. Those anodes that contain a central cavity have one with a diameter of 0.6 inches. A pressure scan from 3.0 to 8.0 torr is performed for each anode. We begin shots first at the pressure we believe to be the optimal neutron producing pressure, based on previous experiments we performed with our DPF. Because these anodes were newly fabricated, the anodes must first be primed by taking a series of initial shots to expel the excess copper on at their tips and therefore, conditioning them for plasma production. These anodes were chosen in attempt to target two physical characteristics of the central anode: its tip shape and the presence or lack of a central cavity. Similar versions of these shapes have been tested before, except that of the flat slit hollow anode. The idea behind this unique design, which has never been used before, is to have a line of sight into the interior of the anodes with hollows. This would allow us to detect plasma activity within the anode which may help explain the dynamics of plasma pinches that occur with a hollowed anode.

Table 2-1. Symbols used to identify each anode in this thesis and their characteristics.

|  | Hollow   | Solid  |
|--|--|--|
| Flat<br>          | <br> | <br> |
| Hemispherical<br> |   |   |
| Flat Slit<br>     |   |   |

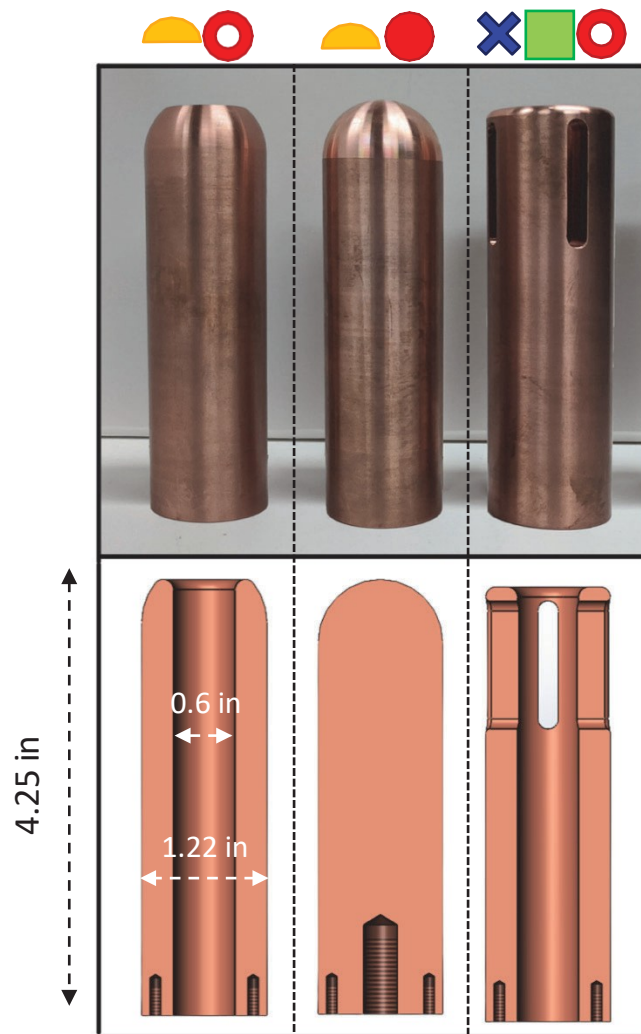


Figure 2-4. The hemispherical hollow, hemispherical solid, and flat top slit hollow anodes along with their defining symbols, CAD drawings, and dimensions. Each anode is made of copper and is 4.25 inches in length and has an outer diameter of 1.22 inches. The hollows have a diameter of 0.6 inches.

## 2.4. Diagnostics

### 2.4.1. Be-activation Detector

Neutron yield was examined using a Beryllium (Be) activation detector which is seen in Figure 2-5. It was designed by Mission Support and Test Services (MSTS) and cross-calibrated at the Ion Beam Lab at Sandia National Laboratory in Albuquerque, NM.



The detector is placed outside of the chamber at an average distance of 14 cm from the pinch and contains a plastic scintillator that holds 12 Be rods. Incident neutrons reach the Be-detector and activate it by creating an alpha particle emission of Be-9 which then results in He-6. He-6 then decays via beta emission in the form of an electron into Li-6 which has a half-life of 806 ms. The photomultiplier tube (PMT) that captures the electrons released in the decay is biased at 15 mV and -2.2 kV with a constant fraction discrimination threshold of the output. A Multichannel Scalar (MCS) processing system is used to collect the Be-detector signals which uses counts that are binned in 160 ms intervals over a range of 8 seconds. This allows us to capture the expected signal background noise and the decay. Each raw half-life count corresponds to  $-1.1 \times 10^6$  neutrons over  $4n$ , and the lower detection limit of neutrons per pulse is  $7.67 \times 10^5$  [12].

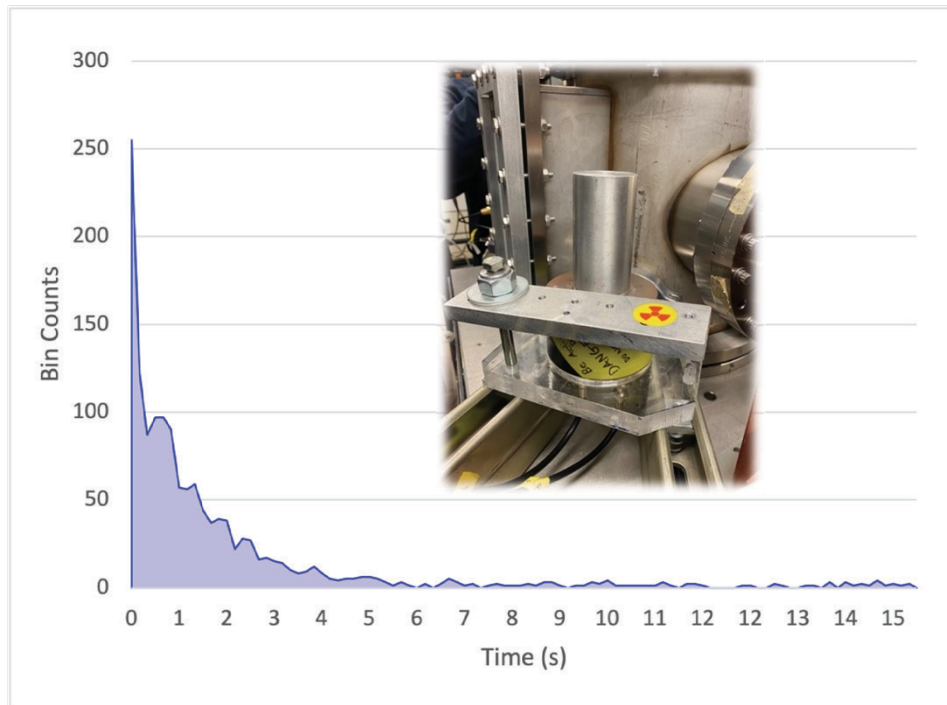


Figure 2-5. Be-activation detector designed by MSTs and cross-calibrated at the Ion Beam Lab in Sandia National Lab and placed directly outside of the vacuum chamber. A graphical example of a decay in bin counts in MCS data is shown.

## 2.4.2. Schlieren and Time Integrated Images

Schlieren and time integrated images were gathered during experiments. In order to obtain Schlieren images for each shot, green lasers with a wavelength of 532 nm were used. These lasers probe the pinch and build the integrated images and Schlieren images. The two cameras used for Schlieren imaging capture the run-down phase of the plasma sheath formation towards the bottom of the anode and the pinch phase at the top of the anode. Delay generators are used to help adjust the timing of the lasers in order to have them go off around the same time as the pinch. Typically, during a round of shots at a particular pressure, the pinch forms around the same time with a  $\pm 0.01 \mu\text{s}$  (in the case where trigger and laser jitter is minimal), which allows us to properly align the laser pulse to the pinch timing. Figure 2-6 shows Schlieren images that can be obtained with our set up which includes images of the rundown phase and the radial implosion phase.

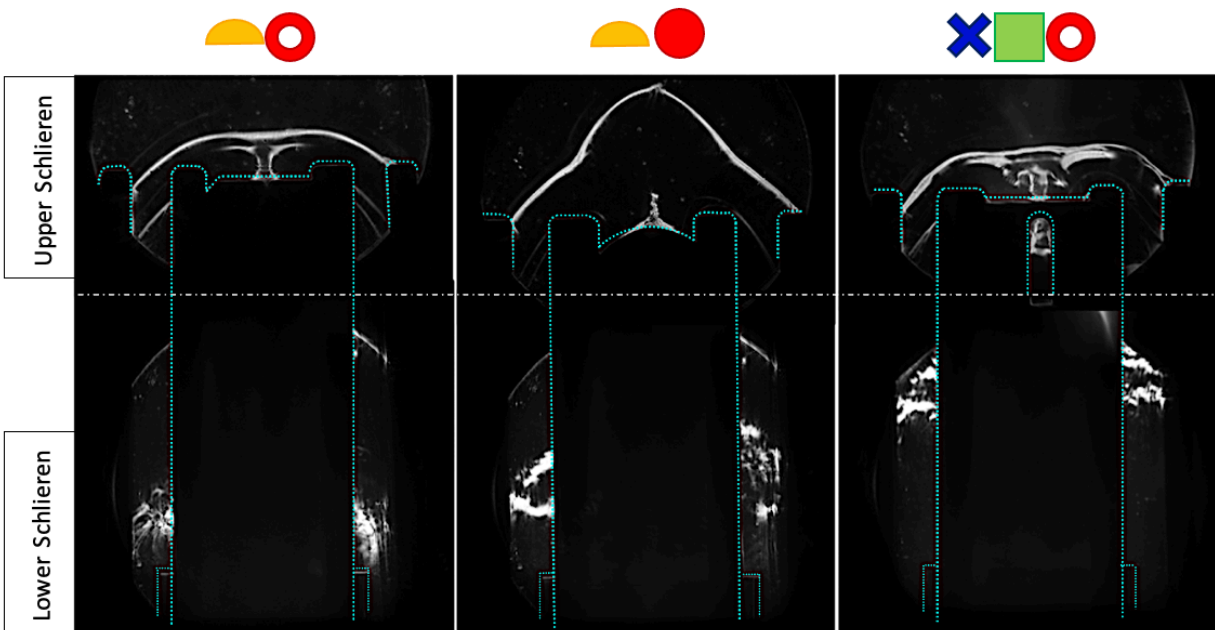


Figure 2-6. "Upper" and "lower" Schlieren images of an experiment for each anode. The "lower" Schlieren image is the rundown phase in which we see the plasma sheath lift off. The upper Schlieren image is that which captures the top of the anode in which the pinch occurs. The anode is outlined to promotes visibility.

### 2.4.3. AXUV Diodes

A pair of AXUV diodes with an area of 20 mm<sup>2</sup> are placed at the top of the chamber in the axial direction of the top of the anode. Another pair of AXUV diodes with a smaller area of 1 mm<sup>2</sup> are placed in the radial direction from the. These diodes were biased to 150 V and were used to measure the soft X-ray emission produced by the various anode configurations. These diodes were cross calibrated using a filter of 45  $\mu\text{m}$  aluminum through a series of shots at optimal neutron producing pressure. For a number of experiments, there was a pair of ross filters were used for both the axial diodes and the radial diodes. These filter pairs were 45  $\mu\text{m}$  Aluminum and 12.5  $\mu\text{m}$  Copper whose transmission curves are shown in Figure 2-7., as well as 10  $\mu\text{m}$  Aluminum and 3  $\mu\text{m}$  Copper.

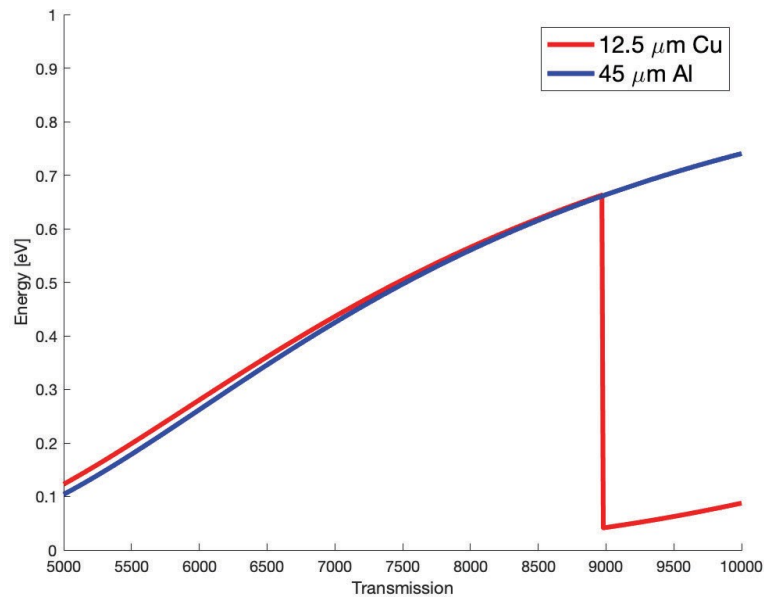


Figure 2-7. Transmission curves for 12.5  $\mu\text{m}$  Cu and 45  $\mu\text{m}$  Al filters from Henke Gas Transmission Website [13].

## 3. Results and Discussion

### 3.1. Neutrons

Hundreds of experiments for each anode took place in order to gather Schlieren images, neutron, and diode data at a pressure range of 3.0 torr to 8.0 torr in intervals of 0.5 torr. The Be-activation detector and MCS system along with a MATLAB code designed to extract the values acquired by the MCS provided absolute neutron yield data. The maximum neutrons and average neutrons for each anode per pressure in torr of deuterium are presented in Figure 3-1. Compared to the other anodes, the hemispherical hollow produced the most neutrons with maximum neutron yield of  $1.97 \pm 0.1 \times 10^8$  at 6.5 torr. This anode is most similar to the converging anode from Hussain [9] and incorporates a hollow similar in diameter to the optimized neutron producing anode in Shaw [8]. Their results support ours and so it is reasonable to say that a rounded or converging anode tip and a hollow enhances neutron production.

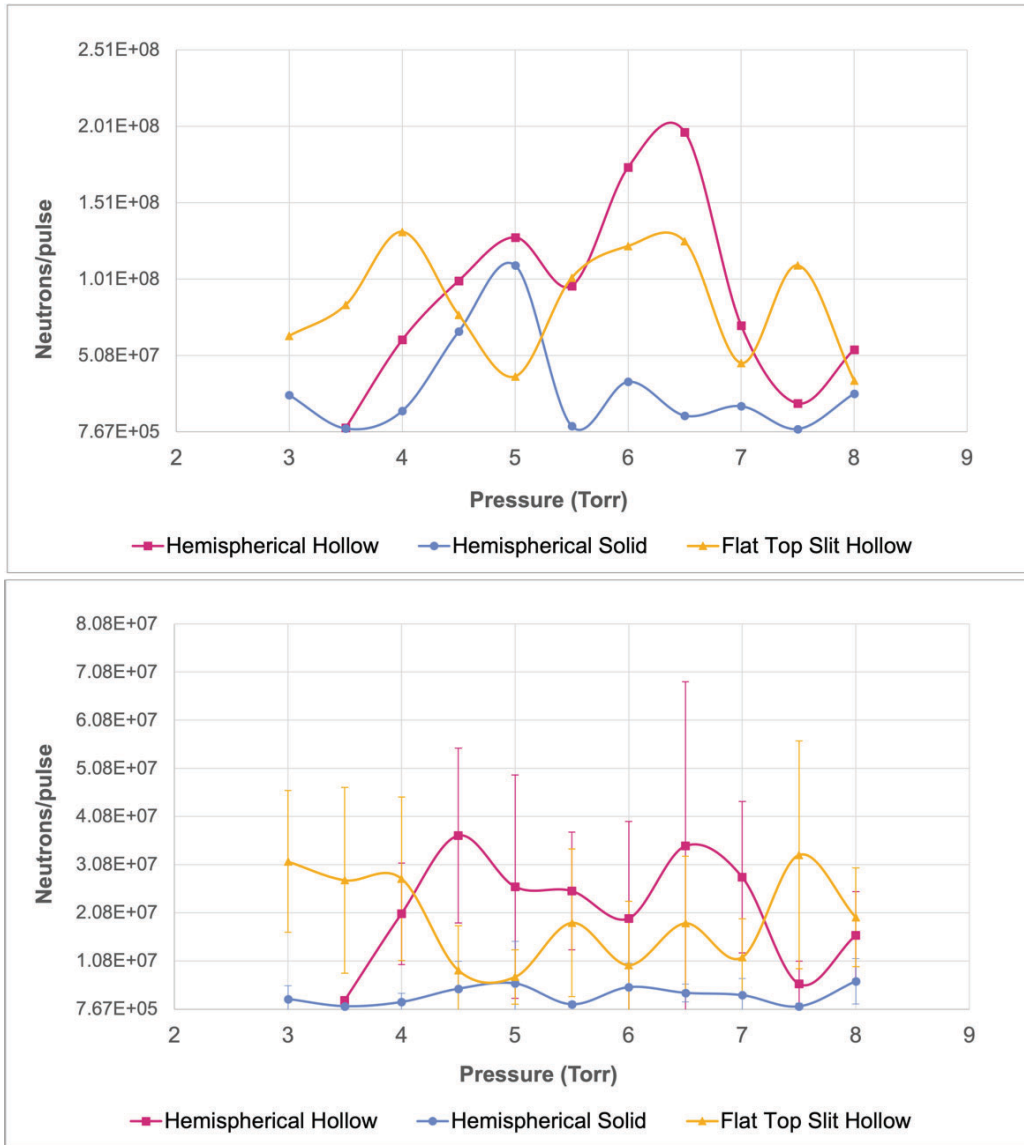


Figure 3-1. Maximum neutron yield per anode (top) at a pressure range from 3 torr to 8 torr as well as their corresponding neutron averages and standard deviations (bottom).

In order to increase the accuracy of the calculated average neutron yield from the collected data, certain shots were disregarded. The neutron averages were taken by removing the data from the shots that had outside influence which caused a lack of neutrons. DPFs need to be primed with a number of shots every day before producing valuable data. For instance, the first shots of the day are meant to "warm up" the system and usually do not produce neutrons. Shots taken after the chamber is open to air also require a series of initial shots to remove the

unwanted elements in the chamber. These experiments did not have valuable data and instead produced neutron and X-ray yield at or below noise level.

We want to compare neutron maximums as well as neutron averages for each anode at each pressure of our scan in order to find trends and substantiate the reproducibility of our neutron data. A significant trend that is seen in our maximum neutron yield data is a dip in neutron yield at 5.5 torr. This is trend that is also seen in previous work done in the same DPF [12] and brings question if DPF presents a bimodal distribution of neutrons or if this is just a case that relates specifically to UCSD's DPF. This trend is common among most of the anodes, however, it is not as clear in the neutron average graph. When comparing the neutron maximum yields to average yields, there are large error bars and differences between the two data sets. There are multiple dips in average neutron yield at pressures that don't align with the with those in the maximum yield analysis. The error bars are also relatively large indicating that there are many outliers which tell us that reproducing these larger neutron yields from Figure 3-1a) is not a simple task and will require an extensive number of shots.

Our neutron data can be compared to a studied recently completed in our lab that studied the effects of insulator sleeve length on neutron yield [12] using a flat top hollow anode. Our study uses the optimized insulator sleeve length found of 3.56 inches which makes our data comparable to those shots that used the same insulator sleeve length. When neutron yields per pressure for our three anodes are compared to the anode from Hahn *et. al*, it is seen that the hemispherical hollow anode produces a higher maximum neutron yield than that of the flat top hollow anode. It also shows a similar trend to that of our dip in maximum neutron yield at 5.5 torr that has been apparent in other studies. Based on these results and the simulations done by

Appelbe and Chittenden, one can conclude that the round tip of the hemispherical hollow anode leads to a cleaner pinch than those with a flat top geometry and without a hollow.

### 3.2. Schlieren and Time Integrated Images

Schlieren and time integrated images were gathered for each of the anodes. The integrated images shown in Figure 3-1 illustrate the brightness of the pinch while the Schlieren images in provide a clear image of the moving plasma sheath and the pinch. Pinch dynamics may serve as a qualitative indicators of potential neutron yields. If a particular shot had a neutron yield that was fairly over the detection limit, the Schlieren images tended to show a structured and dense pinch. However, in order to capture this image, the timing of the cameras had to align or be close to the time of the pinch.

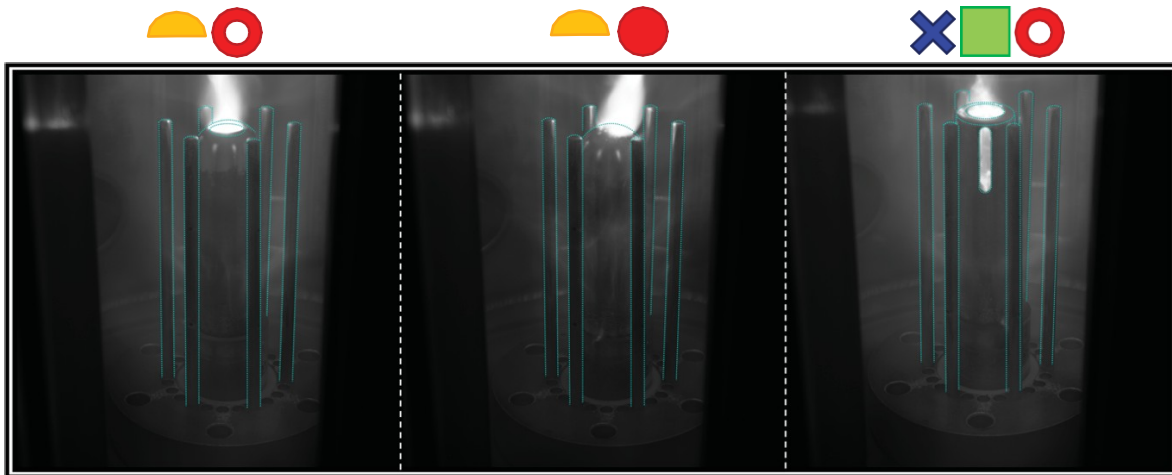


Figure 3-2. Images of a pinch occurring with each anode at a pressure of 5 torr. The pinch that forms with the hollow anodes moves in the axial direction as it is channeled by the hollow. The bright light that forms at the tip of hemispherical solid anode is asymmetric and is believed to be copper ablation. This is corroborated by X-ray data that is for future work on this DPF.

Via our MATLAB script, we were able to track the pinch timing as well as the camera timing for each shot. If needed, the image timing could be shifted in attempt to get it as close to the pinch time as possible. Figure 3-3 shows a series of Schlieren images gathered for each of

the anodes. The top row of images shows what a well-timed pinch looks like for each anode and the corresponding column of images show what the time evolution of the pinch for each anode looks like. One can see the plasma sheath going through the axial, radial, and implosion phases through these images based on the time in which the image was captured. There are various characteristics of the plasma can be observed through these images such as sheath velocity [12] and pinch dynamics. For the latter, one can see the difference between the manner in which the plasma pinches at the top of the anode. For example, the pinch that occurs with the hemispherical hollow anode tends to be smooth and symmetrical, while the hemispherical solid experiences asymmetry and instabilities.





Figure 3-3. Schlieren images of well-timed pinches for each anode as well as corresponding time evolution images. The anode and cathode rods are outlined to improve visibility. The ideal pinch is one that has minimal instabilities and a uniform and dense column is produced at the tip of the anode. The hemispherical solid anode was not able to properly support the production of a stable pinch. The corresponding pressures to each of these well timed pinch shots are shown at the bottom right of each image. For the time evolution images, each of these were different shots taken at the same pressure of 5 torr. Their corresponding neutron yields are found on the top right of each image.

### 3.2.1. Pinch Dynamics

Schlieren imaging allows us to qualitatively analyze the pinch dynamics of each of the anodes. Until now, the pinch dynamics have not been analyzed because there is no line of sight into the inside of the typical hollow anodes used for DPF experiments. Activity inside of the anode would help understand the development of the pinch, which is the goal behind our flat top hollow anode with slits. The concentric slits aspect is a new and unique design that had not been tested until this experiment and allowed us to study plasma dynamics within the hollow. Figure 3-4 shows a close up of anodes during their implosion phase and also shows plasma activity within the hollow through one of the slit openings. The image shows that the pinch is forming inside the anode which is what is expected from the hemispherical hollow anode in which the line of sight into its interior is blocked.

The proof of plasma activity within the anode indicates that the elongated pinch is forming within the anode at the time of implosion due to the extra space for the deuterium gas to seep into. This is not the case, however for the solid anode since it does not have a cavity within itself to allow an elongated pinch to form. The hemispherical solid on the other hand does not have the physical space to allow the pinch to collimate as the other anodes and instead tends to have varying sheath dynamics prone to instabilities. The solid anode tended to act as a copper ablation source and expel more X-rays than the hollow anode.

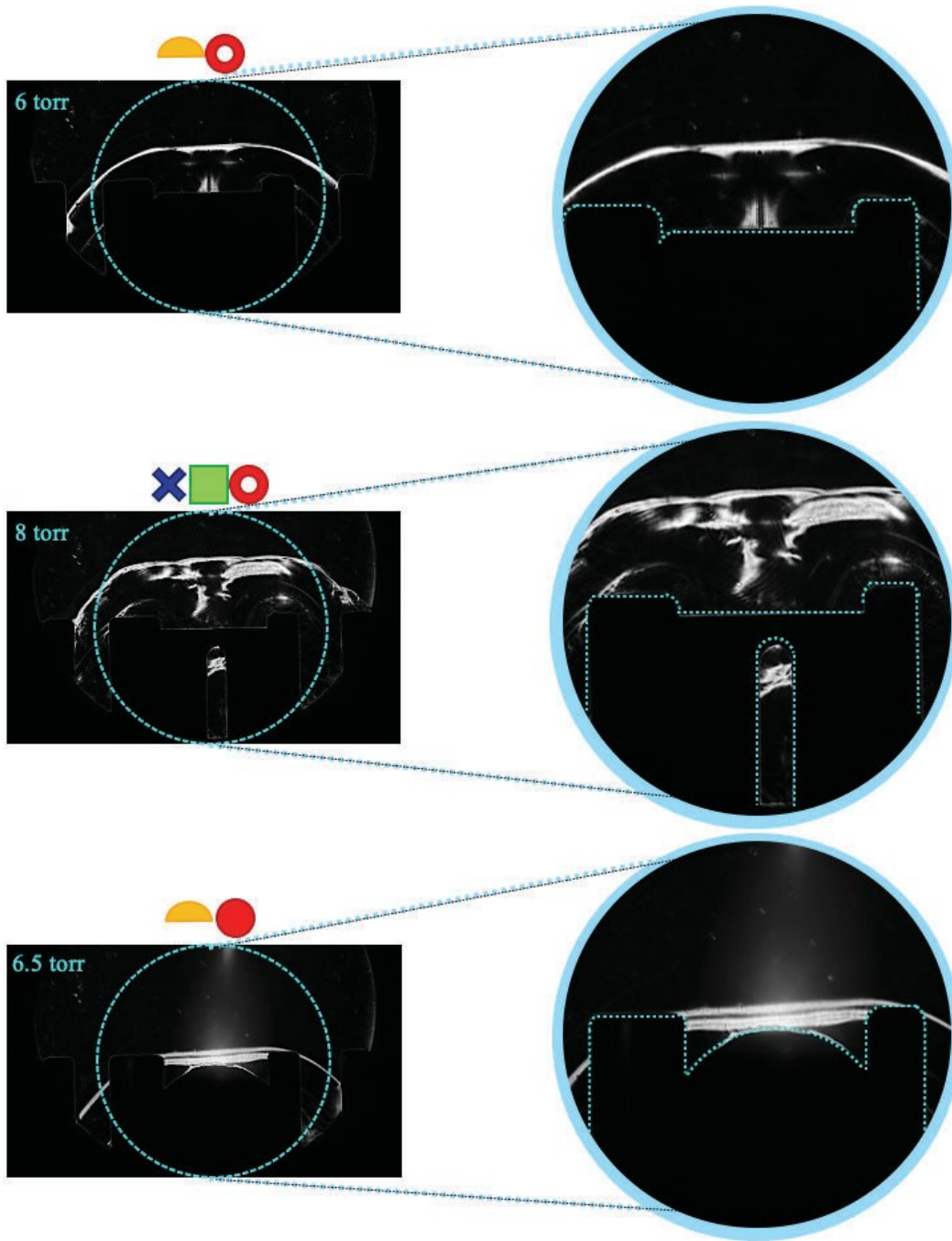


Figure 3-4. Close up images of tip of each anode to see the dynamics of the pinch formation. The hemispherical hollow anode found has a symmetric pinch while the hemispherical solid does not form a pinch. The flat top hollow anode with slits shows plasma activity inside of the hollow. In the close-up image, one can see the pinch extending into the hollow which leads to the conclusion that this is occurring in the hemispherical hollow anode as well.

Based on the neutron yields obtained from each of the anodes and the Schlieren and time integrated images, one concludes that the presence of a hollow is optimal for neutron production. The extension of the pinch inside of the anode along with its neutron yield exemplifies that the hollow is necessary for a long and structured pinch which promotes neutrons. The solid anode on the other hand, ablates copper which in return degrades the pinch and neutron yield. This copper emission would be seen in PIN diode signals which would be an interesting topic for future analysis.

## 4. Conclusions

The correlation between the presence of a hollow in an anode with a hemispherical tip is examined through the means of neutron and X-ray detection and Schlieren imaging. A flat top hollow anode with four concentric slits is introduced in which the slits were designed in order to create a line of sight into the central cavity of those anodes during implosion. This allowed us to capture active plasma activity within the hollow of those anodes that contained them. We were able to observe the pinch occurring within the hollow which was previously theorized. This additional space for deuterium to seep into and allow the pinch to form leads to a collimated pinch which is correlated to a higher neutron yield. The solid anode, however, did not have that space necessary for the pinch to form and therefore was not able to form successful pinches and instead served as an electron beam source which makes it prone to more ablation. The presence of a hollow reduces X-rays and enhances neutrons while the lack of a hollow leads to a uniform X-ray emission on all sides of the anode.

### 4.1. Future Work

In attempt to continue the search efforts started by Appelbe and Chittenden and others to optimize the physical aspects of the DPF anode, more configurations must be tested. This may include anode permutations with different shape configurations as well as different hollow sizes. This thesis as well as other papers have concluded that the presence of a hollow is ideal for neutron production so future studies may put an emphasis on using such anodes and changing other factors. Targeting other aspects of the DPF such as the electrical components by reversing the polarity of the machine may be the next step in building upon this work. Employing new diagnostics such as a HOPG spectrometer would also be beneficial to further

understand the characteristics behind the plasma. Although it was touched upon in our research, an in-depth X-ray study using diodes with ross pair filters would be useful to find the extent of soft X-ray emission and find identify how much copper is ablated for different anodes. These efforts can help further our understanding of fusion and ultimately lead to the ability to harness its energy for an alternate, cleaner energy source.

This thesis, in part is currently being prepared for submission for publication of the material. Eudave, Veronica; Hahn, Eric N.; Valdivia, Maria Pia; Vaughan, Jacquelynne; Ghosh, Swarvanu; Conti, Fabio; Beg, Farhat, N. The thesis author was the primary investigator and author of this material.

## References

- [1] F.F. Chen, Introduction to Plasma Physics and Controlled Fusion, Springer International Publishing, Cham, 2016. <https://doi.org/10.1007/978-3-319-22309-4>.
- [2] M.G. Haines, A review of the dense Z -pinch, Plasma Phys. Control. Fusion. 53 (2011) 093001. <https://doi.org/10.1088/0741-3335/53/9/093001>.
- [3] W.H. Bennett, Magnetically Self-Focussing Streams, Phys. Rev. 45 (1934) 890-897. <https://doi.org/10.1103/PhysRev.45.890>.
- [4] N.V. Filippov, T.I. Filippova, V.P. Vinogradov, DENSE HIGH-TEMPERATURE PLASMA IN A NON-CYLINDRICAL z-PINCH COMPRESSION, Nucl Fusion Suppl. (1962). <https://www.osti.gov/biblio/4731683-dense-high-temperature-plasma-non-cylindrical-pinch-compression> (accessed August 18, 2022).
- [5] J.W. Mather, Characteristics of the Dense Plasma Focus Discharge, Phys. Fluids. 11 (1968) 611. <https://doi.org/10.1063/1.1691959>.
- [6] B. Appelbe, J. Chittenden, Understanding neutron production in the deuterium dense plasma focus, AIP Conf. Proc. 1639 (2014) 9-14. <https://doi.org/10.1063/1.4904765>.
- [7] M. Krishnan, The Dense Plasma Focus: A Versatile Dense Pinch for Diverse Applications, IEEE Trans. Plasma Sci. 40 (2012) 3189-3221. <https://doi.org/10.1109/TPS.2012.2222676>.
- [8] B.H. Shaw, S. Chapman, C.M. Cooper, C. Goyon, J. Angus, A. Link, D.P. Higginson, J.X. Liu, J.M. Mitrani, Y.A. Podpaly, A. Povilus, A. Schmidt, Maximizing neutron yields by scaling hollow diameter of a dense plasma focus anode [Neutron yield maximization and anode surface damage characterization by scaling hollow diameters of a DPF anode], J. Appl. Phys. 124 (2018). <https://doi.org/10.1063/1.5051665>.
- [9] S.S. Hussain, S. Ahmad, G. Murtaza, M. zakaullah, Effect of anode shape on correlation of neutron emission with pinch energy for a 2.7kJ Mather-type plasma focus device, J. Appl. Phys. 106 (2009) 023311. <https://doi.org/10.1063/1.3177253>.
- [10] N. Talukdar, N.K. Neog, T.K. Borthkur, Effect of anode shape on pinch structure and X-ray emission of plasma focus device, Results Phys. 3 (2013) 142-151. <http://doi.org/10.1016/j.rinp.2013.09.001>.
- [11] K.A. Long, N. Moritz, N.A. Tahir, GORDGON – computer code for the calculation of energy deposition and the slowing down of ions in cold materials and hot dense plasmas, Germany, 1983.
- [12] E.N. Hahn, S. Ghosh, V. Eudave, Effect of insulator length and fill pressure on filamentation and neutron production in a 4.6 kJ dense plasma focus, Phys. Plasmas. (2022) 12.

- [13] B.L. Henke, E.M. Gullikson, and J.C. Davis., CXRO X-Ray Interactions With Matter, (n.d.). [https://henke.lbl.gov/optical\\_constants/](https://henke.lbl.gov/optical_constants/) (accessed August 22, 2022).